Nuclear Instruments and Methods in Physics Research A 767 (2014) 83–91

Contents lists available at ScienceDirect

Nuclear Instruments and Methods in Physics Research A

journal homepage: www.elsevier.com/locate/nima

Test of digital neutron–gamma discrimination with four different photomultiplier tubes for the NEutron Detector Array (NEDA)

X.L. Luo [a,b,*], V. Modamio [c], J. Nyberg [b], J.J. Valiente-Dobón [c], Q. Nishada [b], G. de Angelis [c], J. Agramunt [d], F.J. Egea [d,e], M.N. Erduran [f], S. Ertürk [g], G. de France [h], A. Gadea [d], V. González [e], T. Hüyük [d], G. Jaworski [i,j], M. Moszyński [j,k], A. Di Nitto [l], M. Palacz [j], P.-A. Söderström [m], E. Sanchis [e], A. Triossi [c], R. Wadsworth [n]

[a] Department of Instrument Science and Technology, College of Mechatronics and Automation, National University of Defense Technology, Changsha, China
[b] Department of Physics and Astronomy, Uppsala University, SE-75120 Uppsala, Sweden
[c] INFN, Laboratori Nazionali di Legnaro, I-35020 Legnaro, Padova, Italy
[d] IFIC-CSIC, University of Valencia, Valencia, Spain
[e] Department of Electronic Engineering, University of Valencia, E-46071 Valencia, Spain
[f] Faculty of Engineering and Natural Sciences, Istanbul Sabahattin Zaim University, Istanbul, Turkey
[g] Nigde Universitesi, Fen-Edebiyat Falkültesi, Fizik Bölümü, Nigde, Turkey
[h] GANIL, CEA/DSAM and CNRS/IN2P3, Bd Henri Becquerel, BP 55027, F-14076 Caen Cedex 05, France
[i] Faculty of Physics, Warsaw University of Technology, ul. Koszykowa 75, 00-662 Warszawa, Poland
[j] Heavy Ion Laboratory, University of Warsaw, ul. Pasteura 5A, 02-093 Warszawa, Poland
[k] National Centre for Nuclear Research, A. Soltana 7, PL 05-400 Otwock-Swierk, Poland
[l] Johannes Gutenberg-Universität Mainz, 55099 Mainz, Germany
[m] RIKEN Nishina Center, 2-1 Hirosawa, Wako-shi, Saitama 351-0198, Japan
[n] Department of Physics, University of York, Heslington, York YO10 5DD, UK

ARTICLE INFO

Article history:
Received 23 June 2014
Received in revised form
13 August 2014
Accepted 14 August 2014
Available online 22 August 2014

Keywords:
Digital neutron-gamma discrimination
Liquid scintillator
Photomultiplier tube
Charge Comparison
Integrated rise-time
Time-of-flight
NEDA

ABSTRACT

A comparative study of the neutron–γ discrimination performance of a liquid scintillator detector BC501A coupled to four different 5 in. photomultiplier tubes (ET9390kb, R11833-100, XP4512 and R4144) was carried out. Both the Charge Comparison method and the Integrated Rise-Time method were implemented digitally to discriminate between neutrons and γ rays emitted by a ^{252}Cf source. In both methods, the neutron–γ discrimination capabilities of the four photomultiplier tubes were quantitatively compared by evaluating their figure-of-merit values at different energy regions between 50 keVee and 1000 keVee. Additionally, the results were further verified qualitatively using time-of-flight to distinguish γ rays and neutrons. The results consistently show that photomultiplier tubes R11833-100 and ET9390kb generally perform best regarding neutron–γ discrimination with only slight differences in figure-of-merit values. This superiority can be explained by their relatively higher photoelectron yield, which indicates that a scintillator detector coupled to a photomultiplier tube with higher photoelectron yield tends to result in better neutron–γ discrimination performance. The results of this work will provide reference for the choice of photomultiplier tubes for future neutron detector arrays like NEDA.

1. Introduction

Since liquid scintillators, the most widely used detector materials for fast neutron detection, are sensitive to both neutrons and γ rays, the neutron–gamma (n–γ) discrimination is an essential requirement of fast neutron detection in radiation fields where neutrons and γ rays coexist [1]. Over the past few decades various n–γ discrimination methods have been developed based on the principle that the decay rate of the light output of a liquid scintillator depends on the radiation type. Among these methods, the most popular ones are conventional methods such as Charge Comparison (CC) method [2,3] and the Zero-Crossover (ZCO) method [4,5].

A lot of effort has recently been put into the development of n–γ discrimination, with focus on two aspects: the n–γ discrimination method itself and the scintillator material. On one hand, the availability of digital pulse-processing systems not only offers the feasibility of transforming the conventional n–γ discrimination methods into the digital framework, but also opens the possibility of proposing sophisticated n–γ discrimination algorithms. For instance, several original

* Corresponding author at: Department of Physics and Astronomy, Uppsala University, SE-75120 Uppsala, Sweden. Tel.: +46 735673247; fax: +46 184715999.
E-mail address: luo.xiaoliang@physics.uu.se (X.L. Luo).

http://dx.doi.org/10.1016/j.nima.2014.08.023
0168-9002/

digital methods have yielded good results for n–γ discrimination such as the correlation method [6], pulse gradient analysis (PGA) [7–9], artificial neural networks [10–12], fuzzy *c*-mean algorithm [13,14], wavelet algorithm [15–17], and frequency gradient analysis (FGA) [18–21]. On the other hand, some research groups have demonstrated the possibility of manufacturing plastic scintillators with efficient pulse shape discrimination [22]. A new plastic scintillator EJ-299-33 capable of n–γ discrimination has been developed and commercialised very recently [23,24]. Although the n–γ discrimination quality of this plastic scintillator is currently poorer compared to that of liquid scintillators, the plastic scintillator has the advantage of removing the undesirable properties of a liquid scintillator, such as flammability, toxicity, and the necessity of an expansion volume [25].

However, it should be noted that regardless of the scintillator material and the algorithms used, n–γ discrimination would be impossible without a photomultiplier tube (PMT), which converts the light output of a scintillation pulse into a corresponding electrical signal. In this study, the principal task is to investigate the dependence of the n–γ discrimination performance of a liquid scintillator on the PMT type. This issue was evaluated in the context of the construction of the NEutron Detector Array (NEDA) [26–28]. The NEDA project addresses the design of a neutron detector array to be used as an ancillary device for large γ-ray arrays such as AGATA [29,30] using both intense stable as well as radioactive ion beams. The full version of NEDA will consist of around 350 identical hexagonal detectors, each containing about 3 l of liquid scintillator of type BC501A. The scintillators will be coupled to 5 in. PMTs for readout of the scintillation light and the signals will be digitised by electronic modules specifically designed for NEDA [31–33]. Modern neutron detector arrays, such as NEDA, combine two techniques for discrimination of neutrons and γ rays: pulse-shape analysis and time-of-flight (TOF). Both discrimination methods require excellent time resolution, thus, challenging the performance figures of the PMTs to be used. NEDA will consist of many closely packed liquid scintillators in order to achieve a high neutron detection efficiency. Nevertheless, only with an excellent n–γ discrimination performance, it is possible to identify weak reaction channels associated with emission of neutrons. Therefore, the n–γ discrimination performance of a BC501A liquid scintillator detector coupled to four different PMTs: ET9390kb, R11833-100, XP4512 and R4144 (see Table 1) has been tested carefully with the experimental set-up described in Section 2. The initial choice of the PMTs was restricted only to 5 in. PMTs that could meet our demands, such as fast timing, good linearity and large quantum efficiency. The results of n–γ discrimination and related properties of different PMTs are given and discussed in Section 3. Finally, the conclusions arising from this study are stated in Section 4.

2. Experiment

The measurements were carried out at INFN-LNL. The experimental set-up is illustrated in Fig. 1. All four tested PMTs have a diameter of 5 in. and are coupled to the same cylindrical cell containing BC501A scintillator liquid, 5 in. in diameter and 5 in. in depth. The BC501A detector was placed at 50 cm from a ^{252}Cf source to detect the neutrons. The activity of the source was about 2 MBq. The HV was set to get a signal amplitude of about 1 V/MeV for each PMT using a ^{60}Co source. All PMTs were shielded with μ-metal from magnetic fields. A lead brick with a thickness of 5 cm was put between the source and the BC501A detector. This shielding reduced the count rate due to γ rays without losing too many neutrons, thus keeping the count rate of the PMT at a reasonable value of around 2 kHz. In addition a cylindrical 1 in. by 1 in. BaF_2, mounted on a 2 in. PMT R2059, was placed as close as possible to the ^{252}Cf source for detection of γ rays, which provided a time reference for the TOF measurements. A time-to-amplitude (TAC) module was used to measure the time difference between the two detectors, using the coincidence signal (leading edge defined by the BC501A detector) as start and a delayed signal from the BaF_2 detector as stop. The threshold of the constant fraction discriminator (CFD) was set to approximately 30 keVee (keV electron equivalent). The counting rate of the BaF_2 detector was 200 kHz and the coincidence rate was 200 Hz. Signals from both detectors were digitised with a Struck SIS3350 digitiser [34] working at a 500 MHz sampling rate and with 12-bit resolution (effective number of bits $=9.2$). The analogue TAC and coincidence signals were also digitised by a Struck SIS3302 digitiser [35] with 100 MHz sampling rate and 16-bit resolution (effective number of bits ≈ 13). The data acquisition system was triggered by the coincidence signals [36]. In this study, the digital signals from the BC501A detector, together with the TOF information, were used for n–γ discrimination. For each PMT, a total of 100,000 pulse events were analysed in the present work. The total numbers of recorded sampling points were 496 and 488 for SIS3350 and SIS3302, respectively. The baseline shift was removed for each pulse by subtracting the average value of 70 sampling points in the pre-trigger range of the digitised waveform. A small amount of distorted pulses ($<1\%$ of the total), with heavily fluctuating baselines, were discarded.

3. Results and discussion

3.1. Digital CFD and average waveforms

Since the dynamic range of the scintillator pulse amplitude is quite large, a leading edge discriminator would cause a dependence of the trigger time on the pulse amplitude, an effect called time walk [1]. A CFD has been implemented digitally to generate, for each signal, a fixed time after the leading edge of the pulse has reached a constant fraction of the pulse amplitude [28]. The process involves taking the sum of the original signal attenuated to 20% and the delayed and inverted original signal, followed by extracting the point where this sum signal crosses the zero axis.

Table 1
The characteristics of the studied PMTs.

PMT	**ET9390kb**	**R11833-100**	**XP4512**	**R4144**
Manufacturer	ET Enterprises	Hamamatsu	Philips/Photonis	Hamamatsu
Photocathode material	Bialkali	Superbialkali	Bialkali	Bialkali
Photocathode diameter (in.)	5	5	5	5
Quantum efficiency (%)	28	35	24	22
Number of dynode stages	10	8	10	8
Anode pulse rise time (ns)[a]	5	4.3	2.5	1.5
Voltage divider	C636	E6316-01MOD2	VD123K (active)	E7693MOD2

[a] The given values are taken from the datasheets provided by the manufacturers. The anode pulse rise times of the PMTs measured in our experiment are considerably larger than these values, mainly because the PMTs are coupled to a large scintillator [28].

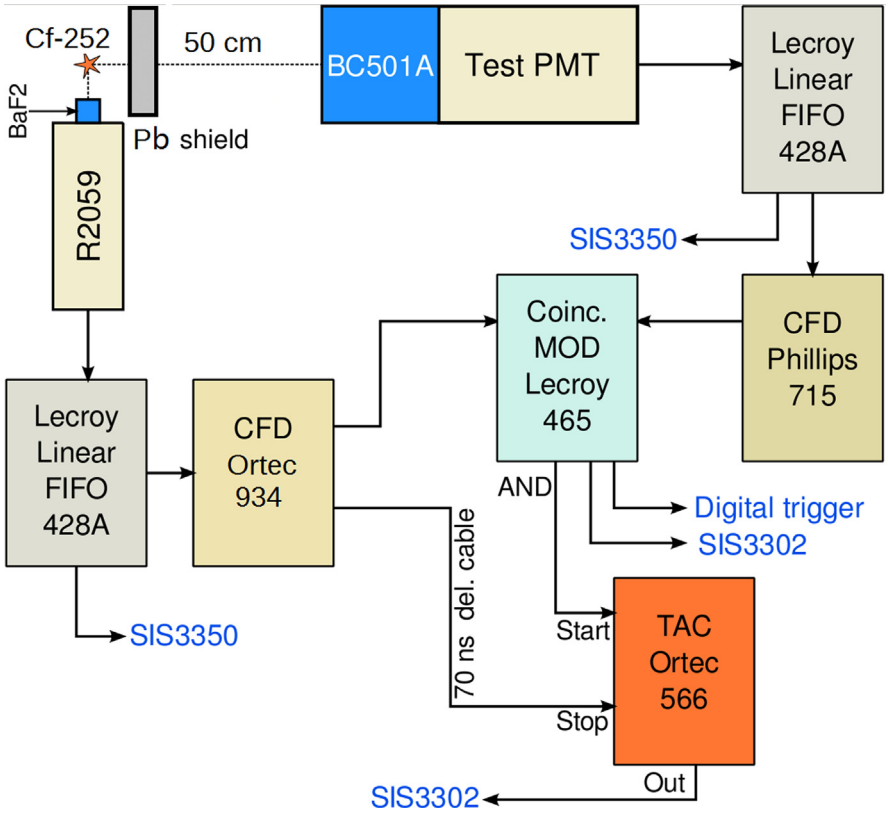

Fig. 1. Block scheme of the experimental arrangement.

This point corresponds to the time at which the original pulse reaches 20% of its final amplitude. This timing reference, which is independent of the peak height, has been used in the n–γ discrimination to accurately determine the integration ranges for each signal. The average waveforms, time-aligned using the digital CFD, for each PMT are shown in Fig. 2. It can be seen that each pulse was triggered at the same time in spite of the different pulse shapes. An obvious slowing down of the pulse measured with ET9390kb was observed, as ET9390kb is a slow PMT for spectroscopy while R11833-100, XP4512 and R4144 are faster. For the pulse measured with R11833-100, a slight increase in signal size at around 90 ns may be due to a non-optimal design of the voltage divider with respect to impedance matching for this tube.

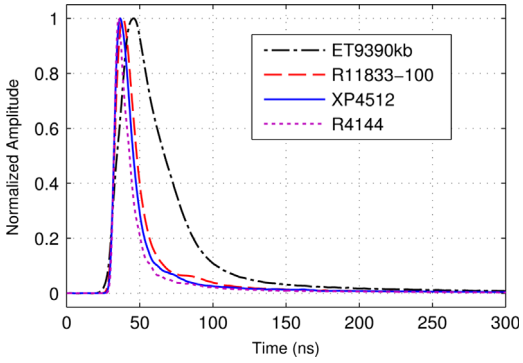

Fig. 2. Average waveforms for PMTs ET9390kb, R11833-100, XP4512, and R4144 (100,000 pulses for each PMT) time-aligned using a digital CFD algorithm.

3.2. Photoelectron yield

The photoelectron yield is of great importance for n–γ discrimination, as the quality of the discrimination is affected by the statistical fluctuation of the number of photoelectrons (Nphe) in the slow component of the scintillation pulse. The Nphe depends on the number of photons per MeV, light collection from the scintillator, and the quantum efficiency of the photocathode. The Nphe per energy unit was measured by comparing the position of the peak corresponding to a single photoelectron to the position of the Compton edge of γ-ray emitted by a ^{137}Cs source [37]. The results of the Nphe measurement for the four PMTs are shown in Table 2. The Nphe per MeV values are relatively low, because the photoelectron yield of large volume scintillators is reduced due to light attenuation inside the scintillator [38].

Table 2
Number of photoelectrons per γ-ray energy deposition for the four different PMTs.

PMT	Nphe/MeV
ET9390kb	1800 ± 90
R11833-100	2070 ± 100
XP4512	1350 ± 70
R4144	950 ± 60

3.3. Energy calibration

The energy calibrations were carried out using four γ-ray sources: ^{241}Am, ^{22}Na, ^{137}Cs and ^{60}Co as listed in Table 3.

Firstly, we got the channel numbers corresponding to energies of the Compton edge or full photon energies of the different γ-ray sources from the measured energy spectra. For our detector, the actual Compton energy value corresponds to around 90% of the peak height on the right side of the Compton distribution according to the simulations performed with Geant4 [26]. The simulations also predict a complete absorption of the 59.5 keV γ rays from ^{241}Am. Moreover, it should be noted that the average energy of the Compton edges was

used for the ^{60}Co source. As shown in Fig. 3, a linear fit was subsequently made of the measured channel numbers versus the electron equivalent energies in keVee for each PMT. These energy calibration results have been used in the digital n–γ discrimination discussed in Section 3.4. Note that the energy mentioned throughout this paper refers to amount of light induced by interactions of neutrons and γ-rays and strictly corresponds only to γ-ray energies, as neutrons produce less light in keVee than their energy in keV.

3.4. Digital n–γ discrimination

In this section, two conventional pulse-shape discrimination methods, the CC method and the integrated rise-time (IRT) method, have been implemented digitally to discriminate neutrons from γ rays. They are based on the principle that the fraction of light that appears in the slow component of the light yield of the liquid scintillators depends on the type of incident particle. In order to quantify the n–γ discrimination performances of the four PMTs, a parameter named figure-of-merit (FOM) was used to evaluate the results of these two pulse-shape discrimination methods in Sections 3.4.1 and 3.4.2. The FOM is defined as [1]

$$\mathrm{FOM} = \frac{S}{\mathrm{FWHM_n} + \mathrm{FWHM_\gamma}} \quad (1)$$

where S is the distance between the neutron and γ-ray peaks in the distribution spectrum of the discrimination parameter, and $\mathrm{FWHM_n}$ and $\mathrm{FWHM_\gamma}$ are their full width at half maximum values. A larger value of FOM normally indicates a better performance of the n–γ discrimination. However, it should be noted that the FOM measures, the degree of separation that can be achieved between different types of event distributions and does not take into account any misidentification cases. This means that in some extreme situations, even a poor n–γ discrimination with a high misidentification rate could still have a fairly large FOM value, though this is unlikely to happen as long as the pulse-shape discrimination method has been implemented properly. For example, the misidentification due to pile-up effects is quite common when the count rate is very high, while the two peaks of the distribution spectrum of the discimination parameter are well seperated, resulting in a large FOM. Therefore, in Section 3.4.3 we have included TOF information to further verify the validities of both the CC method and the IRT method used in this work.

Table 3
Properties of the γ-ray sources used for calibration of the BC501A detector.

Source	γ-ray energy (keV)	Compton edge (keV)
^{241}Am	59.5	–
^{22}Na	511	341
^{137}Cs	662	478
^{60}Co	1253[a]	1041
^{22}Na	1275	1062

[a] The value is the average of 1332 and 1173 keV.

3.4.1. Pulse-shape discrimination by the CC method

The CC method identifies the particle by measuring the integrated charge over two different time regions of the pulse induced by a neutron or γ-ray event. The long integral (total charge) starts from the beginning of the pulse (8 ns before the CFD trigger point) to an optimised end point in the tail, while the short integral corresponding to the slow component is taken from an optimised start point after the pulse peak to the same end point as used for the long integral. The optimal start point of the short integral (t_s) and the end point of both the short and long integrals (t_e) were determined carefully by performing a maximisation of FOM value when leaving both t_s and t_e as free variables. Fig. 4 presents a three-dimensional plot of this process of optimising t_s and t_e using the CC method for PMT ET9390kb at 320 ± 20 keVee as an example. The optimal values of t_s and t_e were set to 90 ns and 300 ns respectively. For t_e, the FOM did not improve for larger values than 300 ns. The value of t_e was kept constant at 300 ns in all cases to ensure as short time interval as possible for minimising pile-up effects. This is reasonable as the intensity of the slow component of the light pulse is quite low beyond 300 ns [39].

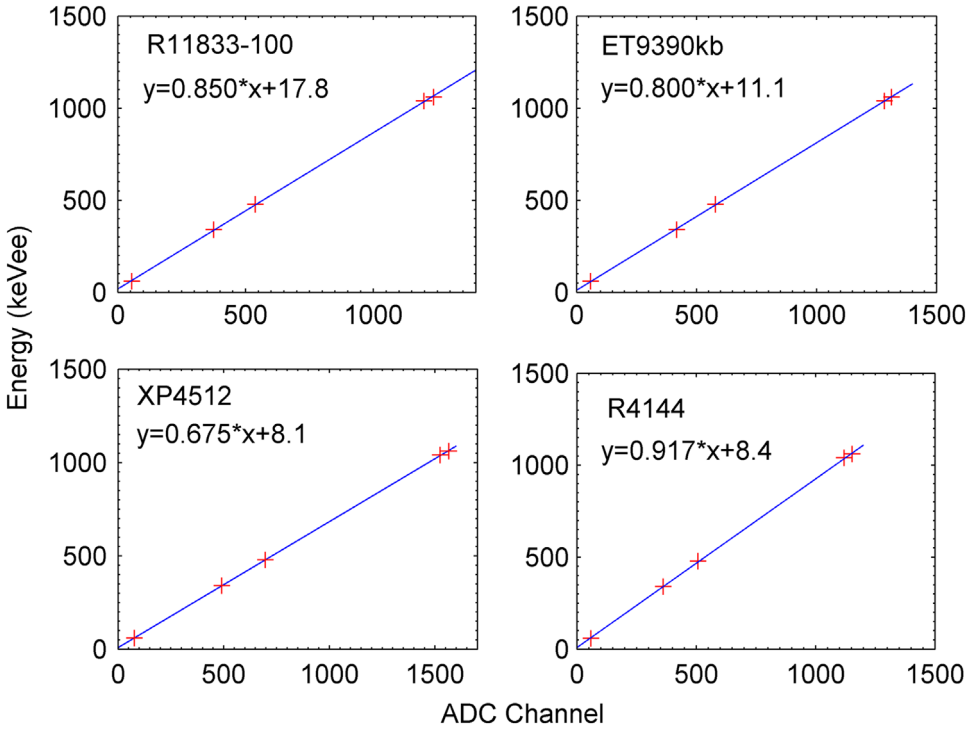

Fig. 3. Energy calibration plots for the four PMTs.

Fig. 5 shows comparison of two-dimensional density plots of short integral versus long integral of each pulse measured with PMT ET9390kb, R11833-100, XP4512 and R4144 using an energy threshold of 100 keVee. It can be observed that even with such a large scintillator an effective separation between neutron and γ-ray events has been accomplished down to 100 keVee for each PMT. Since the relative intensity of the slow component of the pulse arising from neutrons (recoil protons) is larger than that of γ rays (electrons), the events located in the upper distribution in Fig. 5 are identified as neutrons while the lower distribution corresponds to γ rays according to the CC method.

Furthermore, we evaluated the n–γ discrimination performance as a function of energy by employing different energy windows between 50 keVee and 1000 keVee in order to get a more quantitative comparison of the discrimination capability. Fig. 6 presents the n–γ discrimination spectra, which are the distributions of the ratios of short to long integrals being measured at 320 ± 20 keVee for the different PMTs. Gaussian functions were used to fit the distributions with the curve fitting tool available in MATLAB [40]. The FOM values were then extracted from these Gaussian fits for all the PMTs by applying Eq. (1). The optimal t_s and the extracted FOMs are shown in the legends of Fig. 6.

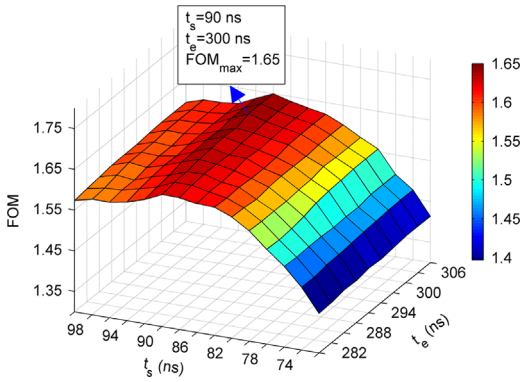

Fig. 4. FOM values measured for PMT ET9390kb at 320 ± 20 keVee as a function of t_s and t_e used in the CC method.

Additionally, the FOMs in different energy regions ranging from 50 keVee to 1000 keVee for all PMTs have been obtained in the way as shown in Fig. 6. Comparison of the measured FOMs of the CC method for each tested PMT is shown in Fig. 7. As seen in Fig.7, the FOM values rise gradually with increasing energy as expected for all PMTs. ET9390kb and R11833-100 generally perform best in terms of n–γ discrimination with only slight difference in FOM values. The PMT XP4512 is slightly worse than R11833-100 and ET9390kb, while R4144 gives considerably lower FOMs compared to other PMTs, indicating its poorest n–γ discrimination capability. This trend of FOMs for different PMTs qualitatively agrees with the measured number of photoelectrons per MeV (Table 2). The error of FOM was calculated based on Eq. (1) by propagating the errors of the parameters derived from the non-linear iterative curve fit.

3.4.2. *Pulse-shape discrimination by the IRT method*

The IRT method can be seen as a digital implementation of the analogue Zero-Crossover (ZCO) method since the integrated rise time can be evaluated directly by digital signal processing rather than first shaping it to extract the ZCO time. The rise time, defined here as the time difference between the point when the integrated pulse crosses a lower fraction and an upper fraction of its maximal amplitude, is used as a parameter to distinguish neutrons from gamma rays. The optimisation of lower and upper points was performed in the same way as for

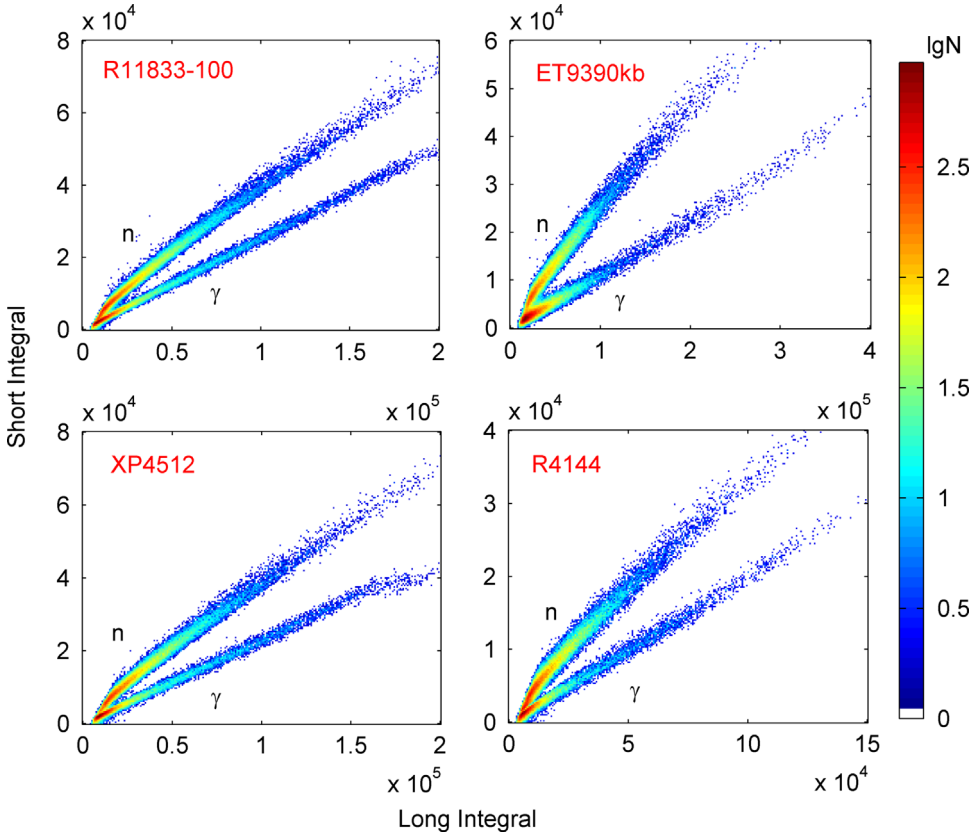

Fig. 5. Density plots of short integral versus long integral of each pulse measured with PMT ET9390kb, R11833-100, XP4512 and R4144 with an energy threshold of 100 keVee.

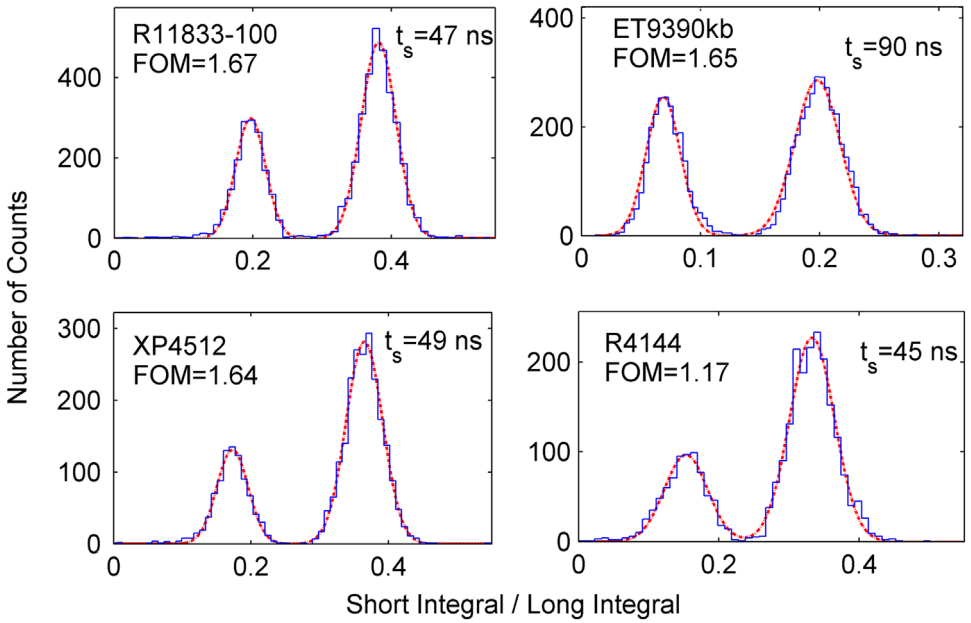

Fig. 6. Neutron–γ discrimination spectra with fitted Gaussian distributions at 320 ± 20 keVee using the CC method for PMT ET9390kb, R11833-100, XP4512 and R4144.

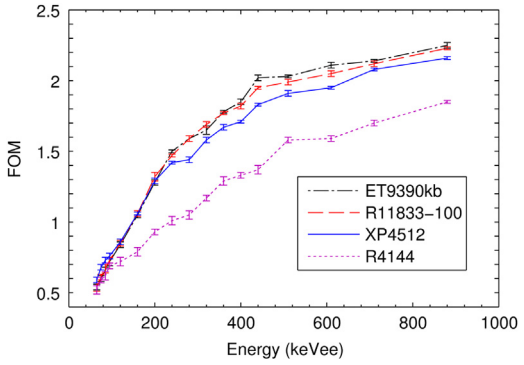

Fig. 7. FOM values of the CC method for PMT ET9390kb, R11833-100, XP4512, and R4144 as a function of energy window (the widths of the windows are 10, 40, and 100 keVee in energy regions of 50–100, 100–500 and 500–1000 keVee, respectively).

the CC method as illustrated in Fig. 4. The optimal values of lower and upper points for PMT ET9390kb, R11833-100, XP4512 and R4144 were found to be 10–92%, 11–86%, 10–84% and 12–87% respectively. The principle of the IRT method is that the integrated rise time of the neutron-induced pulse is longer than that of the γ-ray induced pulse.

Conventionally, the performance of an n–γ discrimination method can be assessed qualitatively by plotting the amplitude of a given pulse against its discrimination parameter [7–9,18,19,41]. Fig. 8 presents comparison of two-dimensional density plots of amplitude against the integrated rise time of each pulse measured with PMT ET9390kb, R11833-100, XP4512 and R4144 using an energy threshold of 100 keVee. In each plot of Fig. 8, the events on the right hand were identified as neutrons and the left groups of events were regarded as γ rays.

Like the CC method, the n–γ discrimination quality was assessed as a function of energy for each PMT. Fig. 9 presents the n–γ discrimination spectra which are the projections of the integrated rise time being measured at 320 ± 20 keVee for the different PMTs. As seen in Fig. 9, the FOMs for each PMT have been extracted with Gaussian fits of the two peaks of the distribution curve corresponding to the γ-ray and neutron events.

Fig. 10 presents a quantitative comparison of the IRT discrimination performance of each PMT in terms of FOM in different energy regions between 50 keVee and 1000 keVee. It can be observed that the trend of FOMs of the IRT method for different PMTs is basically consistent with that of the CC method. Nevertheless, the FOMs of IRT method for R11833-100 are slightly higher than those for ET9390kb, while in the CC method ET9390kb is a little better regarding FOM values. Since these differences are insignificant when taking into account the error of the FOM values, it can be safely concluded that R11833-100 and ET9390kb have the best capabilities of n–γ discrimination. In general, the IRT method performs slightly better than the CC method over most of the energy range for all PMTs, with the FOM values on average about 7%, 4%, 3% and 6% higher for PMT R11833-100, ET9390kb, XP4512 and R4144, respectively. This is probably because the IRT method can cancel out part of the high-frequency noise present in the signal by integrating the pulse. Yet at the same time, it should be noted that the FOMs of different PMTs under 100 keVee are quite similar, all suggesting deterioration in n–γ discrimination performance at low energy. This results from the fact that the signal-to-noise ratio of the low energy signals is quite low due to the scintillation statistics and due to the electronic noise and the quantisation effects of the digitiser, which is a fundamental limitation for any discrimination method [42].

3.4.3. *TOF verification of n–γ discrimination*

Neutrons and γ rays can often be distinguished with a high accuracy by measuring their TOF between the emission point and the detector. Thus, the TOF parameter was used here combined with both the CC method and the IRT method to evaluate their discrimination quality on a qualitative basis. Fig. 11 presents the TOF distribution of the pulses measured with PMT XP4512. Density plots of the n–γ discrimination parameter of the CC method and the IRT method versus the TOF measured with the PMT XP4512 are shown in Figs. 12 and 13 respectively. Two distinct clusters of events are clearly visible as areas of higher density centred at TOF values of ~0 and ~0.38, which correspond to γ rays and neutrons respectively. This indicates that the n–γ discrimination results of both the CC method and the IRT method are similar to that of TOF measurement, which has demonstrated qualitatively the correctness of our implementation of these two methods in Sections 3.4.1 and 3.4.2.

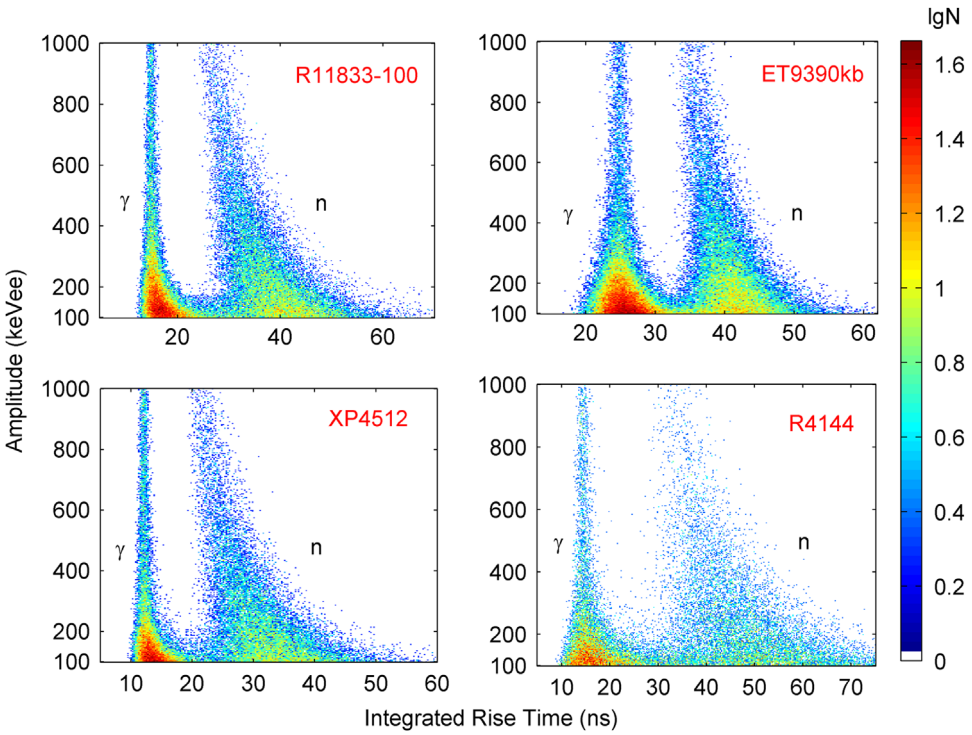

Fig. 8. Density plots of amplitude versus the integrated rise time of each pulse measured with PMT ET9390kb, R11833-100, XP4512 and R4144 with an energy threshold of 100 keVee.

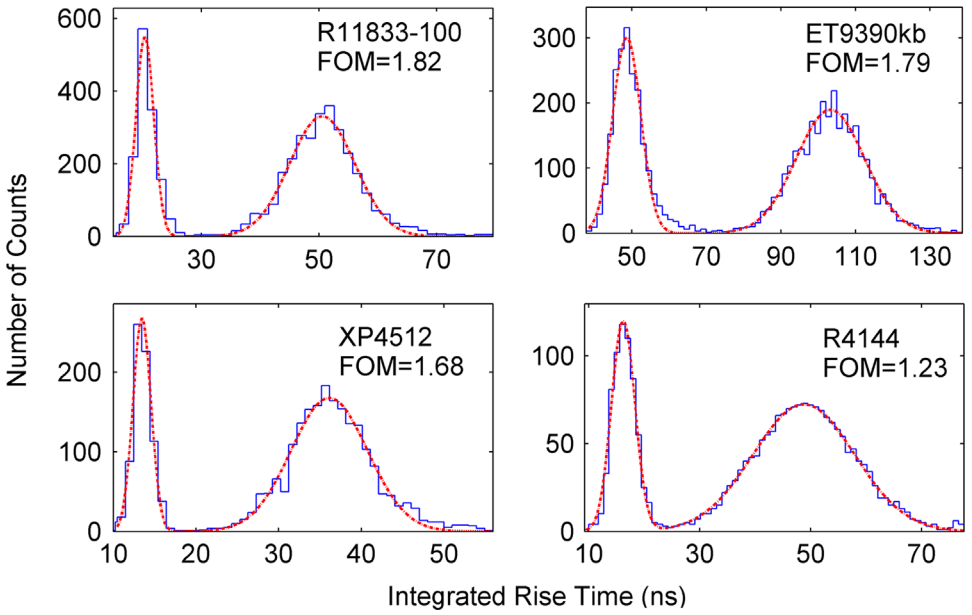

Fig. 9. Neutron–γ discrimination spectra with fitted Gaussian distributions at 320 ± 20 keVee using the IRT method for PMT ET9390kb, R11833-100, XP4512 and R4144.

However, there are some other events located elsewhere in Figs. 12 and 13, most of which are random and pile-up events. In Fig. 13, for instance, random events are mainly distributed parallel to the TOF axis. The TOF method failed to classify these events because TOF measurements require a time reference that is unavailable for them, whereas the IRT method can discriminate them based on the pulse shape. Moreover, the region with an integrated rise time larger than ≈ 20 ns and TOF of about 0 mostly contains pile-up events, because they tend to have longer integrated rise time, which results in the discrepancy between the n–γ discrimination results of the TOF method and the IRT method. The reason for the invalidation of the IRT method in discriminating these events is that the original pulse shape has to some extent been distorted by pile up. Therefore, it is suggested that if available in a real experiment, pulse-shape discrimination and TOF measurement should complement each other to acquire relatively pure neutrons or γ rays.

4. Summary and conclusions

In summary, a comparative study was made with four different PMTs (ET9390kb, R11833-100, XP4512 and R4144) with a diameter of 5 in. regarding the n–γ discrimination performances when coupled to

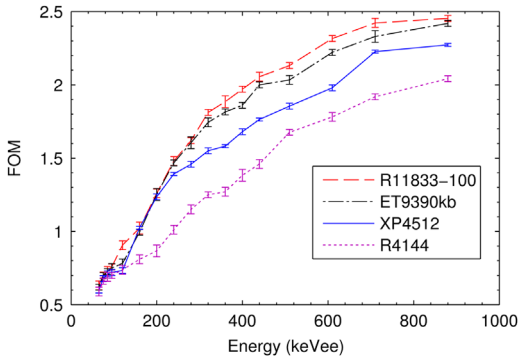

Fig. 10. FOM values of the IRT method for PMT ET9390kb, R11833-100, XP4512, and R4144 as a function of energy window (the widths of the windows are 10, 40, and 100 keVee in energy regions of 50–100, 100–500, and 500–1000 keVee, respectively).

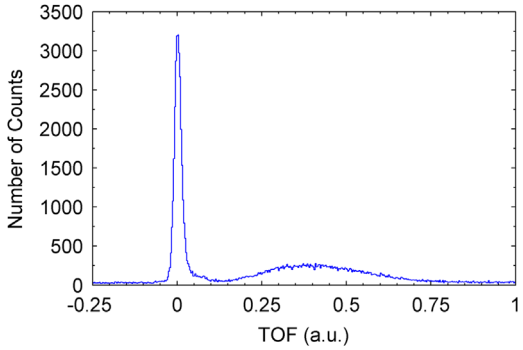

Fig. 11. TOF spectrum of the pulses measured with PMT XP4512.

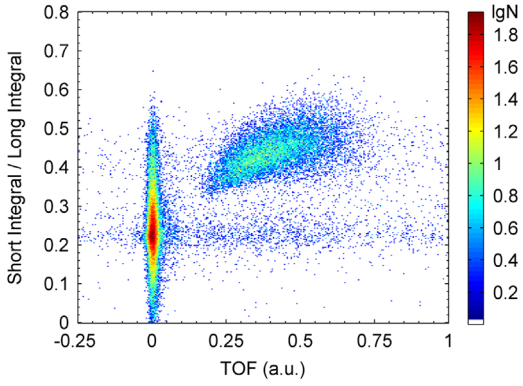

Fig. 12. Density plot of the discrimination parameter of the CC method versus the TOF of each pulse measured with PMT XP4512. No energy threshold was set in the analysis.

the same liquid scintillator detector, with a size of 5 in. in diameter and 5 in. in depth. The analysed waveforms were acquired with an experimental set-up that comprised a ^{252}Cf source, a BC-501A detector and a SIS3530 digitiser with a sampling rate of 500 MHz and with 12-bit resolution. Firstly, the average waveforms as well as the photoelectron yield were measured and an energy calibration was made for each PMT. Secondly, both the CC method and the IRT method were implemented digitally to discriminate neutrons from γ rays. The FOM parameters were evaluated as a function of energy to quantitatively compare the n–γ discrimination properties of the four PMTs. Finally, the n–γ discrimination results were verified by combining the TOF measurement with both the CC method and the IRT method. The results suggest that an effective n–γ discrimination can be achieved down to 100 keVee by all four PMTs. In general, PMT R11833-100 and ET9390kb have the best n–γ discrimination capabilities with only

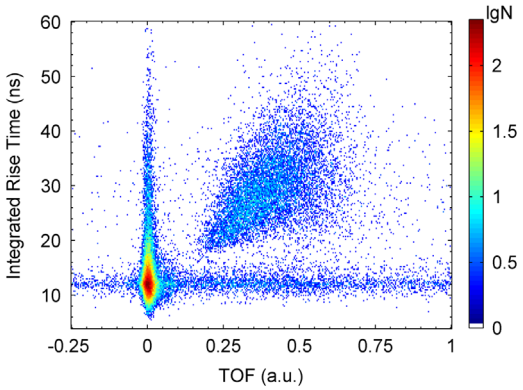

Fig. 13. Density plot of the discrimination parameter of the IRT method versus the TOF of each pulse measured with PMT XP4512. No energy threshold was set in the analysis.

slight difference in FOM values between them. The surprising result that the slow PMT ET9390kb can accomplish the n–γ discrimination as well as the fast PMT R11833-100 is likely because the timing property of ET9390kb is sufficiently good for n–γ discrimination. Therefore, the results are more associated with their relatively higher photoelectron yield per energy unit, which indicates that a scintillator detector coupled to a PMT with higher photoelectron yield can result in better n–γ discrimination performance.

The results of the presented measurement of the pulse-shape discrimination performance of the four PMTs as well as other factors, such as time-resolution and cost, will all be taken into consideration when determining the best PMT to be used for NEDA. Furthermore, the conclusion concerning the n–γ discrimination performances of different PMTs can also provide reference for other modern multi-detector experiments where PMTs are needed to be coupled to scintillators.

Acknowledgements

This work was partly funded by the Swedish Research Council, by the UK STFC, and by the Generalitat Valenciana, Spain, under Grant PROMETEO/2010/101, and by MINECO, Spain, under Grants AIC-D-2011-0746, FPA2011-29854 and FPA2012-33650. X. L. Luo acknowledges the support of the Chinese Scholarship Council (CSC).

References

[1] G.F. Knoll, Radiation Detection and Measurement, fourth ed., Wiley, New York, 2010.
[2] F.D. Brooks, Nuclear Instruments and Methods in Physics Research 4 (1959) 151.
[3] J.M. Adams, G. White, Nuclear Instruments and Methods in Physics Research 156 (1978) 459.
[4] T.K. Alexander, F.S. Goulding, Nuclear Instruments and Methods in Physics Research 13 (1961) 244.
[5] M. Roush, M.A. Wilson, W.F. Hornyak, Nuclear Instruments and Methods in Physics Research 31 (1964) 112.
[6] N.V. Kornilov, V.A. Khriatchkov, M. Dunaev, A.B. Kagalenko, et al., Nuclear Instruments and Methods in Physics Research Section A 497 (2003) 467.
[7] B.D' Mellow, M.D. Aspinall, R.O. Mackin, M.J. Joyce, A.J. Peyton, Nuclear Instruments and Methods in Physics Research Section A 578 (2007) 191.
[8] M.D. Aspinall, B.D' Mellow, R.O. Mackin, M.J. Joyce, et al., Nuclear Instruments and Methods in Physics Research Section A 583 (2007) 432.
[9] M.J. Joyce, M.D. Aspinall, F.D. Cave, K. Georgopoulos, Z. Jarrah, IEEE Transactions on Nuclear Science 57 (2010) 2625.
[10] G. Liu, M.D. Aspinall, X. Ma, M.J. Joyce, Nuclear Instruments and Methods in Physics Research Section A 607 (2009) 620.
[11] N. Yildiz, S. Akkoyun, Annals of Nuclear Energy. 51 (2013) 10.
[12] E. Ronchi, P.-A. Söderström, J. Nyberg, et al., Nuclear Instruments and Methods in Physics Research Section A 610 (2009) 534.

[13] D. Savran, B. Loher, M. Miklavec, M. Vencelj, Nuclear Instruments and Methods in Physics Research Section A 624 (2010) 675.
[14] X.L. Luo, G. Liu, J. Yang, in: Proceedings of the 1st International Conference on Pervasive Computing, Signal Processing and Applications, PCSPA 2010, IEEE, 2010, p. 994.
[15] Y. Yun, G. Liu, J. Yang, X.L. Luo, et al., Chinese Physics C 38 (2014).
[16] S. Yousefi, L. Lucchese, M.D. Aspinall, Nuclear Instruments and Methods in Physics Research Section A 598 (2007) 551.
[17] D.I. Shippen, M.J. Joyce, M.D. Aspinall, IEEE Transactions on Nuclear Science NS-57 (2010) 2617.
[18] G. Liu, M.J. Joyce, X. Ma, M.D. Aspinall, IEEE Transactions on Nuclear Science NS-57 (2010) 1682.
[19] J. Yang, X.L. Luo, G. Liu, et al., Chinese Physics C 36 (2012) 544.
[20] G. Liu, X.L. Luo, J. Yang, et al., Chinese Physics C 37 (2013).
[21] G. Liu, J. Yang, X.L. Luo, et al., Radiation Measurements 58 (2013) 12.
[22] Zaitseva, B.L. Rupert, et al., Nuclear Instruments and Methods in Physics Research Section A 668 (2012) 88.
[23] S.A. Pozzi, M.M. Bourne, S.D. Clarke, Nuclear Instruments and Methods in Physics Research Section A 723 (2013) 19.
[24] D. Cester, G. Nebbia, L. Stevanato, et al., Nuclear Instruments and Methods in Physics Research Section A 735 (2014) 202.
[25] A.L. Hutcheson, D.L. Simonson, M. Christophersen et al., in: Proceedings of Chemical, Biological, Radiological, Nuclear, and Explosives (CBRNE) Sensing XIV, SPIE, 2013, p. 117.
[26] G. Jaworski, M. Palacz, J. Nyberg, et al., Nuclear Instruments and Methods in Physics Research Section A 673 (2012) 64.
[27] T. Hüyük, et al., Conceptual Design of the Neutron Detector Array (NEDA) and an early implementation of NEDA with AGATA, submitted to European Physical Journal, in preparation.
[28] V. Modamio, J.J. Valiente-Dobón, et al., Digital pulse-shape techniques applied to the NEDA neutron-detector array, Nuclear Instruments and Methods in Physics Research Section A, submitted for publication.
[29] S. Akkoyun, A. Algora, B. Alikhani, et al., Nuclear Instruments and Methods in Physics Research Section A 668 (2012) 26.
[30] A. Gadea, E. Farnea, J.J. Valiente-Dobón, et al., Nuclear Instruments and Methods in Physics Research Section A 654 (2011) 88.
[31] F.J. Egea, E. Sanchis, V. González, et al., IEEE Transactions on Nuclear Science NS-60 (2013) 3526.
[32] F.J. Egea, E. Sanchis, V. González, et al., A digital front-end electronics for the neutron detector NEDA, IEEE Transactions on Nuclear Science, submitted for publication.
[33] F.J. Egea, V. González, A. Gadea, et al., A New Front-End High-Resolution Sampling Board for the New-Generation Electronics of EXOGAM2 and NEDA Detectors, IEEE Transactions on Nuclear Science, submitted for publication.
[34] ⟨http://www.struck.de/sis3350.htm⟩ 2014.
[35] ⟨http://www.struck.de/sis3302.htm⟩ 2014.
[36] V. Modamio, et al., LNL Annual Report 2012, 2013, p. 78.
[37] M. Moszyński, G. Costa, G. Guillaume, B. Heusch, A. Huck, et al., Nuclear Instruments and Methods in Physics Research Section A 308 (1991) 97.
[38] M. Moszyński, G. Bizard, G.J. Costa, D. Durand, et al., Nuclear Instruments and Methods in Physics Research Section A 317 (1992) 262.
[39] M. Moszyński, G.J. Costa, G. Guillaume, et al., Nuclear Instruments and Methods in Physics Research Section A 350 (1994) 226.
[40] MathWorks, ⟨http://www.mathworks.com⟩.
[41] K.A.A. Gamage, M.J. Joyce, N.P. Hawkes, Nuclear Instruments and Methods in Physics Research Section A 642 (2011) 78.
[42] X.L. Luo, Y.K. Wang, G. Liu, J. Yang, et al., Nuclear Instruments and Methods in Physics Research Section A 717 (2013) 44.